D.-Z. Sun, B. Voss*, and W. Schmitt**

Numerical Prediction of Ductile Fracture Resistance Behaviour based on Micromechanical Models

REFERENCE Sun, D.-Z., Voss, B., and Schmitt, W., **Numerical prediction of ductile fracture resistance behaviour based on micromechanical models**, *Defect Assessment in Components – Fundamentals and Applications*, ESIS/EGF9 (Edited by J. G. Blauel and K.-H. Schwalbe) 1991, Mechanical Engineering Publications, London, pp. 447–458.

ABSTRACT A damage model introduced by Gurson and modified by Needleman and Tvergaard was implemented in the finite element code ADINA. After solving various numerical problems and utilising measurable physical parameters like the distribution of inclusions and the void volume fraction at rupture, this model was used to simulate the behaviour of smooth and notched round tension bars. By matching the calculated load drop with the experimentally observed failure strain the critical void volume fraction f_c could be obtained. It turns out that the critical value f_c is fairly independent of the notch radius. Thus, it may be assumed that the effects of the stress triaxiality are well covered by the model. The same set of parameters as obtained from the tension test was used to simulate the experimental load–displacement and J_R curves of a sidegrooved CT specimen. A satisfactory agreement of prediction and experiment could be found if a proper material dependent distance l_c was introduced into the numerical simulation. For different cracked specimen configurations reasonable J_R curves were predicted on the basis of the damage model using the same parameters as for the CT specimen.

Introduction

In numerous cases ductile fracture can be characterised by global failure criteria, as the J-integral or the crack tip opening displacement CTOD. However, these single-parameter criteria do not take into account micromechanical aspects, local inhomogeneities, and the stress triaxiality. Obviously, the geometry dependence of J_i values and J_R curves is connected with this fact. Many authors **(1)(2)** have shown that the geometry dependence of fracture toughness makes the application of global fracture criteria difficult, especially for complex geometries and loadings. Recently a series of micromechanical models based on the concepts of continuum damage mechanics have been established to find alternatives.

One of the new methods for ductile fracture analysis has been developed by Needleman and Tvergaard **(3)** on the basis of the yield condition suggested by Gurson **(4)**. In this material model the plastic flow is influenced by microscopic voids which are represented by a single parameter, the void volume fraction. Numerical investigations of this modified Gurson model **(5)(6)** show that the development of microscopic damage and global plastic deformation are well described by the model. A major advantage of this type of micromechanical or damage models is that without using additional numerical techniques the initiation and propagation of the crack occur naturally when the local softening due to the void growth results in the formation of a region

* Fraunhofer-Institut für Werkstoffmechanik, Wöhlerstr. 11, D-7800 Freiburg, FRG.

transmitting only zero stresses. However, most of the published numerical work simulates the processes of ductile rupture by void nucleation and growth without considering a characteristic microstructural distance l_c. In addition, in the literature the practical methods to determine the essential damage parameters for the numerical models were not discussed in detail.

In this work the Gurson model in connection with the microscopic models for ductile fracture was implemented into the finite element program ADINA. The relevant material dependent damage parameters were determined from smooth tensile specimens and were compared with those from the notched bars. Using the damage model, the influence of the critical microstructural distance on the crack extension in a CT-specimen was investigated systematically. The predicted local and global behaviour for various specimen geometries was checked by means of accompanying experiments.

Modified Gurson model

The basis for the modified Gurson model is a plastic potential applicable to porous solids given by

$$\phi = \frac{3\sigma'_{ij}\sigma'_{ij}}{2\sigma_m^2} + 2q_1 f^* \cosh\left(\frac{\sigma_{kk}}{2\sigma_m}\right) - \{1 + (q_1 f^*)^2\} = 0 \tag{1}$$

with σ_m = flow stress of the material. The parameter q_1 was introduced by Tvergaard (7) to improve the prediction of the Gurson model at small f values. f^* is a function of the void volume fraction f. For $f^* = 0$ the plastic potential (1) is obviously identical with that of von Mises. If f^* reaches the limit $1/q_1$ the material loses its load carrying capacity because all stress components have to vanish in order to satisfy equation (1). According to Needleman and Tvergaard the nucleation of new voids and the growth of existing voids were introduced into the Gurson constitutive relations by the following definition of the growth rate of f

$$\dot{f} = \dot{f}_{\text{nucleation}} + \dot{f}_{\text{growth}} \tag{2}$$

$$\dot{f}_{\text{nucleation}} = B(\dot{\sigma}_m + \dot{\sigma}_{kk}/3) + D\dot{\varepsilon}_m^p \tag{3}$$

$$\dot{f}_{\text{growth}} = (1-f)\dot{\eta}_{kk}^p \tag{4}$$

where $\dot{\eta}_{ij}^p$ is the plastic part of the strain rate tensor and ε_m^p is the equivalent plastic strain.

The first part in equation (3) models void nucleation controlled by the maximum normal stress at the phase boundary particle/matrix and the second part models void formation from the equivalent plastic strain ε_m^p. The parameters B and D were chosen under the assumption that void nucleation follows a normal distribution (8). For void formation controlled only by strain, the

coefficient D may be described by

$$D = \frac{f_N}{S_N\sqrt{(2\pi)}} \exp\left[-\frac{1}{2}\left(\frac{\varepsilon_m^p - \varepsilon_N}{S_N}\right)^2\right], \quad B = 0 \tag{5}$$

with f_N = volume fraction of void forming particles, ε_N = mean strain for void nucleation, S_N = corresponding standard deviation. Equation (4) is given by the condition of plastic incompressibility of the matrix material.

The effect of the void coalescence on the plastic deformation was modelled by substituting for f as in the original Gurson model by f^*

$$f^* = \begin{cases} f & f \leqslant f_c \\ f_c + f_{uc}(f - f_c) & f \geqslant f_c, \quad l \geqslant l_c \end{cases} \tag{6}$$

The modelling of the void coalescence is active when the critical void volume fraction f_c is exceeded over a critical distance l_c. The value of the constant f_{uc} can be derived by setting the void volume fraction at final failure f_f in equation (6), $(f^*(f_f) = 1/q_1)$

$$f_{uc} = (1/q_1 - f_c)/(f_f - f_c) \tag{7}$$

The l_c-value is a characteristic parameter of a material which may be related to the mean spacing of void forming inclusions. Figure 1 shows schematically the distributions of the void volume fraction f ahead of a crack tip for three different loading levels. The void growth is accelerated only if f exceeds f_c over a critical distance l_c (curve 2). Since the stress-carrying capacity vanishes for

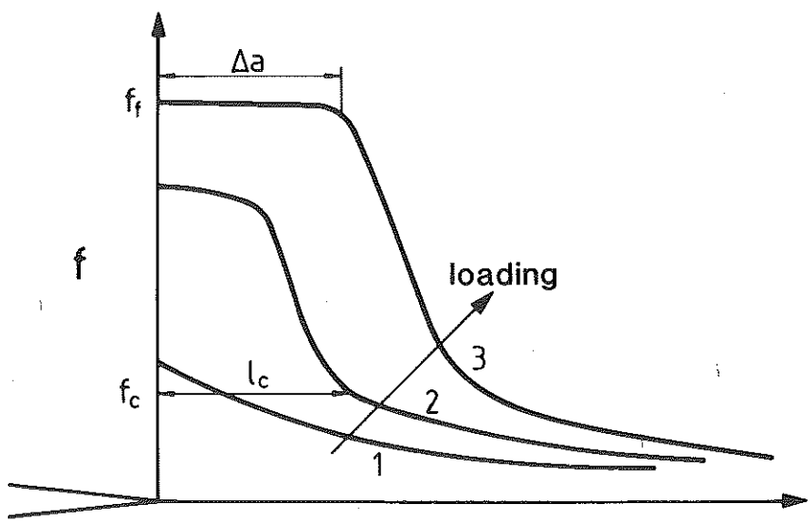

Fig 1 Schematical description of the introduction of l_c-value in the modified Gurson model

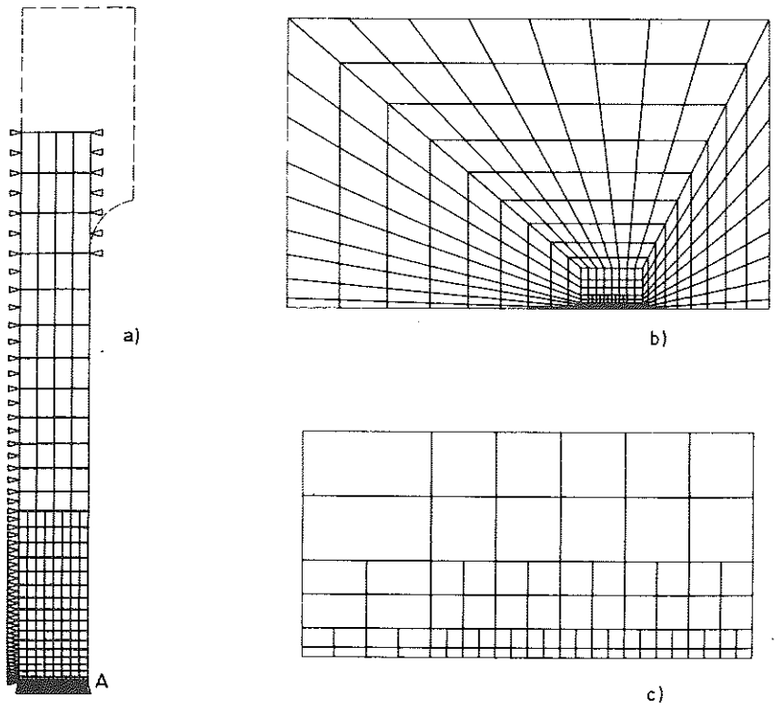

Fig 2 FE-meshes of the investigated specimens (a) round smooth bar. (b) Compact tensile specimen. (c) Section of crack tip region of CT specimen

$f = f_f$, the crack extension Δa can be identified with the size of the region with $f = f_f$ (curve 3).

The following constitutive relations can be derived from the condition $\dot{\phi} = 0$ using the above equations and some additional assumptions **(9)**

$$\dot{\eta}^p_{ij} = \frac{1}{H}\left(\frac{3\sigma'_{ij}}{2\sigma_m} + \alpha\delta_{ij}\right)\left(\frac{3\sigma'_{kl}}{2\sigma_m} + \beta\delta_{kl}\right)\overset{\nabla}{\sigma}_{kl} \tag{8}$$

with $\overset{\nabla}{\sigma}_{kl}$ = Jaumann stress rate tensor.

The parameters H, α, and β are short notations of some long terms derived from the consistency equation for plastic flow **(10)**.

Numerical method

The modified Gurson model was implemented into the finite element program ADINA based on spatial orthogonal coordinates. The inclusion volume determined by quantitative optical microscopy was used as the initial void volume in the numerical simulation ($f_0 = 0.00057$). The void nucleation during the plastic deformation was assumed to be controlled by strain, i.e. $B = 0$. This

assumption ensures that the stiffness matrix does not become unsymmetric. The parameter D was calculated using $\varepsilon_N = 0.3$, $S_N = 0.1$ taken from **(3)** and $f_N = 0.004$ determined for the steel ASTM A 710. As proposed by Tvergaard **(7)** $q_1 = 1.5$ was used. As shown in the equations (6) and (7), the modelling of the void coalescence is affected by both parameters f_c and f_f. For the investigated steel $f_f = 0.15$ was determined by quantitative metallography in a statistical manner from specimens which were unloaded and sectioned close to the onset of failure. The value $f_c = 0.03$ was obtained by fitting the sudden drop in the load versus diameter change curve for a smooth bar. In order to avoid numerical instability problems the constitutive relations described in section 2 were used until f^* reached the value $0.9/q_1$ (instead of $1/q_1$). Subsequently, the failed material was modelled with the constant value $f^* = 0.9/q_1$.

Figure 2 shows the finite element meshes for the smooth bar (Fig. 2(a)) and for the CT specimen (Fig. 2(b) and (c)). The radial deformation in the top region of the smooth bar was restricted by boundary conditions to get necking in point A. The constraint in the top region is caused by the thicker threaded end (Fig. 2(a)). The mesh for the CT specimen was generated with homogeneous element size in the crack tip region. The element length on the ligament from the crack tip up to a distance of 4 mm was 0.1 mm. 8-noded isoparametric elements with two-by-two integration were used. Plane strain conditions were assumed. To account for the large changes in specimen geometry the 'updated Lagrangian' formulation was used and stiffness reformation and equilibrium iterations were applied in every load step.

Results

Simulation of the smooth bar

Since the smooth axisymmetric tensile specimen is most widely used to characterise the material properties, it was attempted in this work to apply the damage models to the smooth bar for determination of transferable damage parameters. In Fig. 3 the experimental load versus diameter change curve (curve 1) was compared with the numerical curves based on two different material models and two different stress–strain curves. Curve 2 was calculated based on the von Mises law with the conventional true stress versus true strain curve, and curve 3 was determined with the same material law, but with the stress–strain curve modified according to Bridgman **(11)**. Figure 3 shows that after the maximum load the curve calculated with the conventional stress–strain data lies above the experimental curve. The reason is that the multiaxiality of the stress state in the necking region is not considered in the conventional evaluation.

An important step for the numerical description of the plastic deformation in the smooth bar is the simulation of the necking which occurs at maximum load during the displacement controlled test. In Fig. 4 the specimen contour

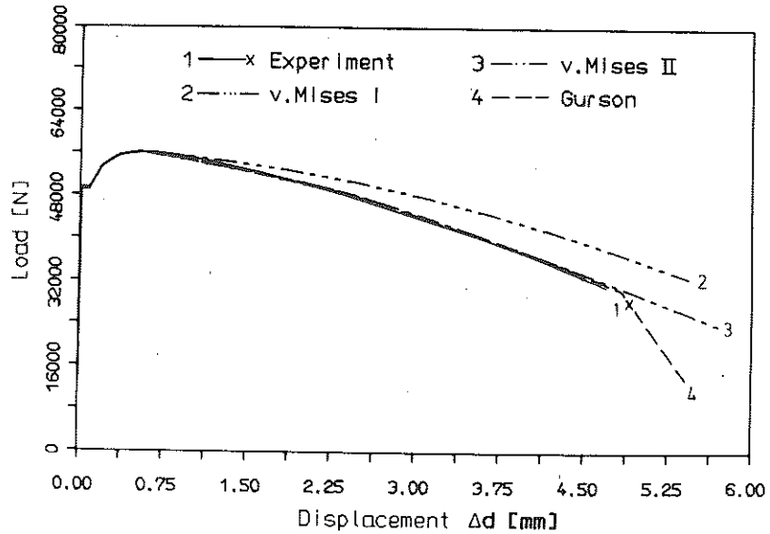

Fig 3 Comparison between numerical and experimental load-diameter change curves for a smooth bar

calculated using the stress–strain curve corrected according to Bridgman was compared with the contour photographed during the experiment for the same loading ($\Delta d = 4.2$ mm) close to the rupture. In the necking region an excellent agreement between the numerical and the experimental results was found.

Figures 3 and 4 make clear that a correction of the stress–strain curve according to Bridgman is sufficient for a satisfactory numerical simulation. With regard to these results all other calculations in this work were performed with the stress–strain curve modified according to Bridgman. Figure 3 also shows that the differences between the von Mises law and the Gurson model are negligible almost up to the rupture of the smooth bar. After a critical

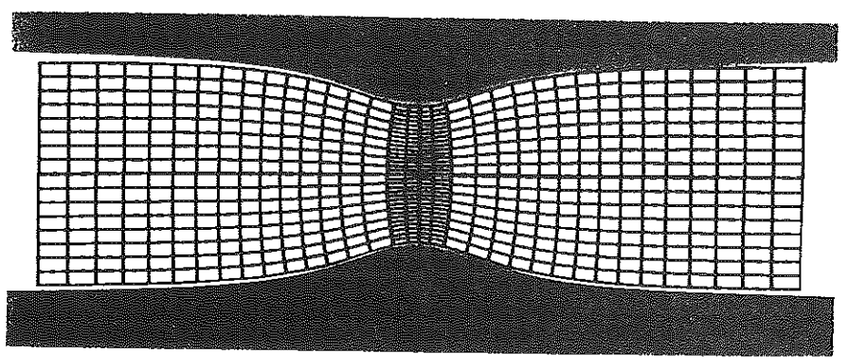

Fig 4 Comparison between numerically simulated and photographed necking of a smooth bar

point, where the void coalescence begins, the differences between both material models increase strongly. The sudden drop of the load–displacement curve caused by crack initiation can only be simulated by a material model including damage (e.g., the Gurson model) (curve 4 in Fig. 3).

Figure 5 shows the distribution of the void volume fraction f for the smooth bar computed with the Gurson model over the cross section of the specimen in the plane of symmetry for different load levels expressed by different Δd-values (change of diameter). The broken lines apply to load steps where the critical value $f_c = 0.03$ is locally exceeded. The damage model predicts that for a smooth bar damage starts in the centre of the specimen. This result is proved by the accompanying experiments. The voids grow slowly before f reaches the critical value f_c. After exceeding the f_c value the void volume fraction f increases rapidly and finally remains at the constant value $f_f = 0.15$.

Figure 6 shows the distribution of the computed von Mises equivalent stress in the smallest cross-section of the smooth bar for different load levels. Prior to achieving the critical amount of damage (solid-lines) the stress distribution based on the Gurson model is similar to that obtained with the von Mises law. As soon as the critical value f_c is exceeded, the equivalent stress predicted with the Gurson model begins to drop, and with increasing deformation the equivalent stress and all stress components approach zero. The length of the damage zone where the equivalent stress is practically equal to zero ($f = f_f$) was used to define the crack extension Δa. An important point to mention is that the distributions of both f and the equivalent stress at the cross-section are very uniform and therefore the critical distance l_c needs not be introduced into the

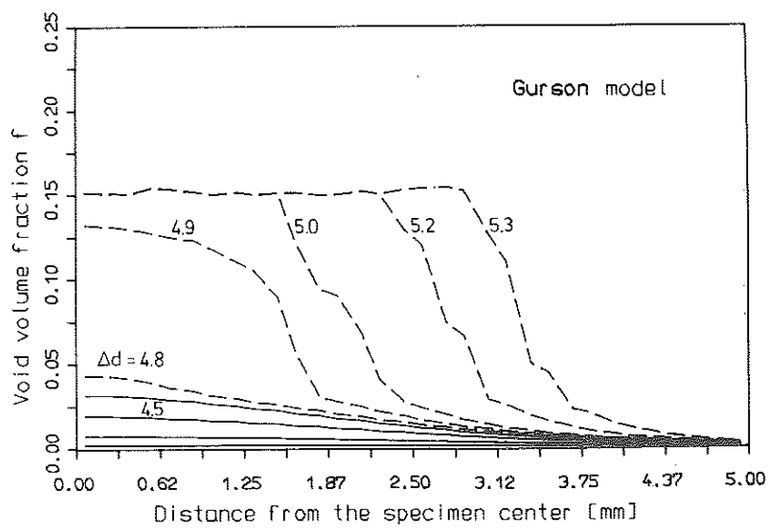

Fig 5 Distribution of void volume fraction in a smooth bar

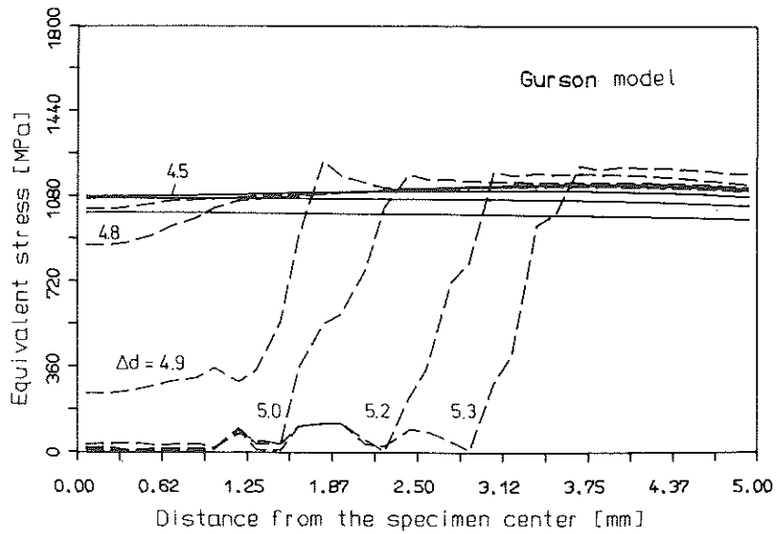

Fig 6 Distribution of equivalent stress in a smooth bar

simulation of the smooth bar. This makes the determination of the f_c value much easier.

Simulation of the notched bars

To investigate the influence of the stress state on the growth and the coalescence of voids, two notched bars with notch radii 0.25 mm and 4 mm were simulated using all parameters determined with the smooth bar. Figure 7 shows for both notch radii the force versus diameter change curves from the numerical analysis and the experiments. The good agreement between the predicted and the experimental onsets of the load drop implies that the effects of the strain constraint on the void growth are well covered by the damage model, and the critical value f_c seems to be almost independent of the stress state. The predictions of the local behaviour of both specimens were strongly supported by the experiments **(10)(12)**.

Application of the damage parameters to cracked specimens

To check the universality of the Gurson model all parameters used for the numerical simulation of the tensile bars were also applied to analyse the compact specimen. Figure 8 shows the computed distribution of the void volume fraction f ahead of the crack tip for different load levels. A comparison between Fig. 8 and Fig. 5 indicates that due to the large variation of the stress–strain field at the crack tip the curves of the distribution of f for the CT-specimen are much steeper than the curves for the uncracked tensile specimens. It is expected that without an introduction of a critical microstructural distance, l_c, a much lower fracture resistance behaviour would be predicted for the CT-specimen. In Fig. 9 the effect of the l_c-value on the computed load–displacement curve is shown. Curve 2 and curve 3 were calculated using the

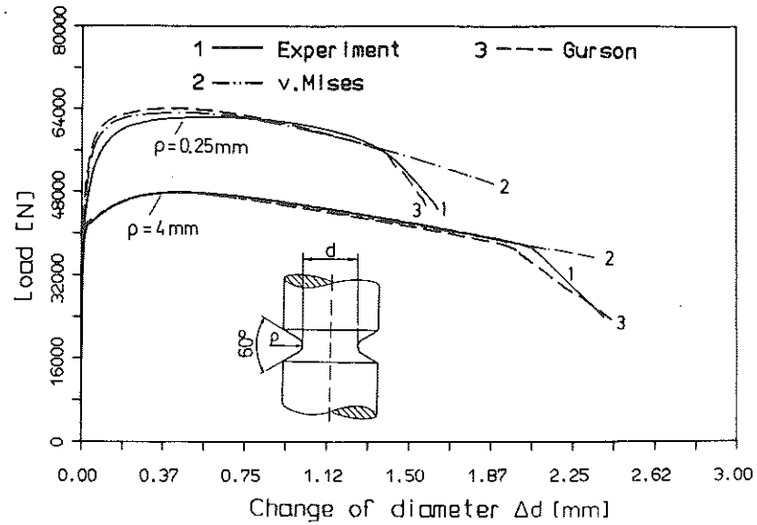

Fig 7 Comparison between numerical and experimental load–diameter change curves for notch radii 4 mm and 0.25 mm

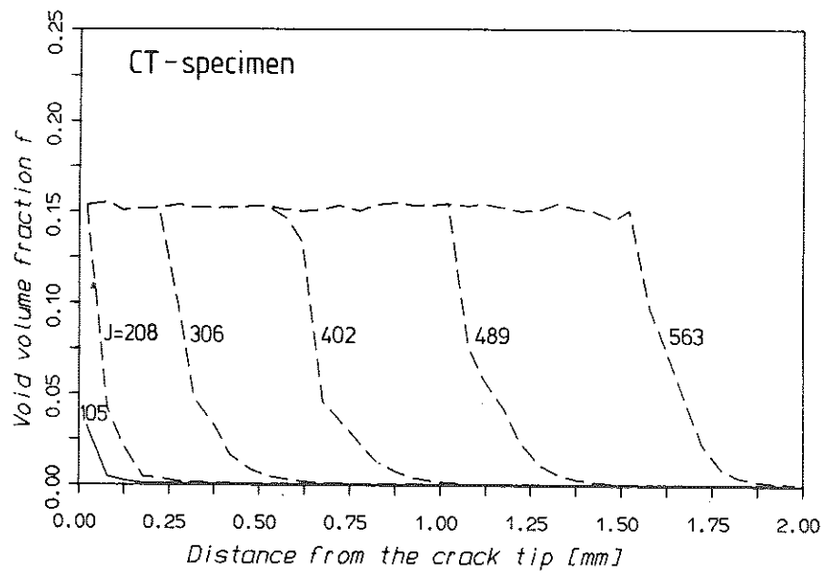

Fig 8 Distribution of void volume fraction ahead of the crack tip of a CT specimen

same mesh with an original element size of 0.1 mm but different l_c-values. It has to be mentioned that with increasing plastic deformation the element size at the crack tip decreases and at the crack initiation it becomes smaller than the lowest l_c-value 0.075 mm. Figure 9 shows that in this case the doubling of the l_c-value results in only a slight rise of the load–displacement curve. The reason is that due to the singular strains, the f-values in the first element have reached the limit value $1/q_1$ ($\sigma_{ij} = 0$) before f exceeds f_c over the distance l_c corresponding to several element lengths. Curve 4 was simulated using the same l_c-value as for curve 3 but only half of the element size. A distinctly lower load–displacement curve caused by an earlier crack initiation was computed for the finer mesh, because the decreasing of the crack tip element size leads to an increasing of the calculated stresses, strains, and void volume fraction and hence to the earlier void coalescence. The analysis of the results in Fig. 9 leads to the conclusion that the defomed element size should be identified with the l_c-value, if only one variable is to be used to cover the effects of both the mesh size and the l_c-value.

In Fig. 10 the J-resistance curve determined from the numerical analysis based on the Gurson model with mesh 1 and $l_c = 0.075$ mm was compared with the experimental curve for the CT-specimen. Using all parameters determined from the smooth bar and the additional parameter l_c the fracture resistance behaviour of the CT-specimen was predicted in quite a satisfactory way.

To study the sensitivity of the damage model to predict J–R curves of different specimens, two other specimen configurations with the same crack length a and specimen width, W, were simulated using the same element size and

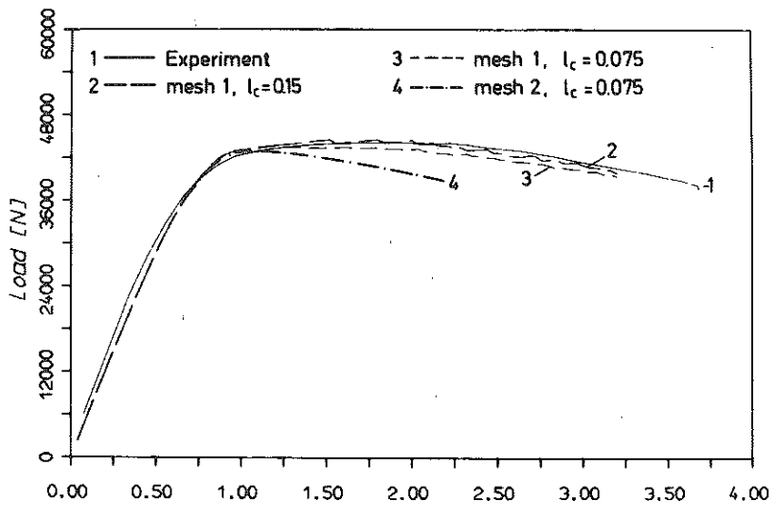

Fig 9 Comparison between numerical and experimental load–displacement curves for a CT specimen

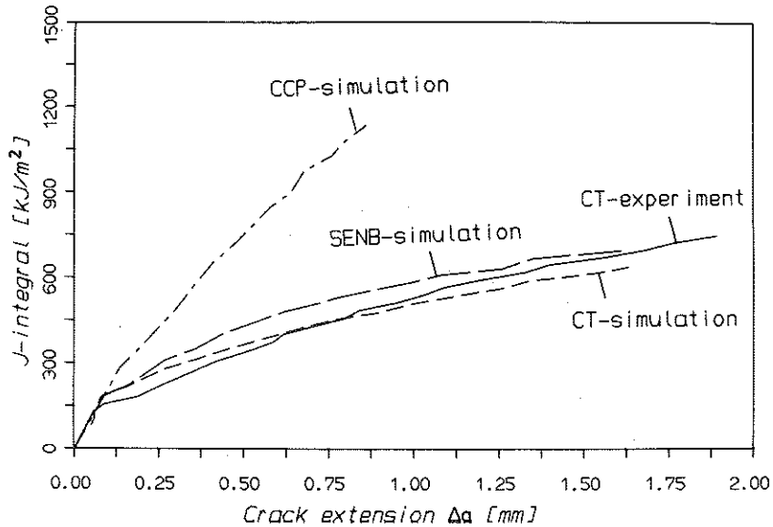

Fig 10 Comparison between the J_R curves predicted for different specimen configurations and the J_R curve determined from CT specimen

parameters as applied for the CT-specimen. Figure 10 shows that the J_R curve simulated for the centre cracked panel (CCP) is much steeper than that of the compact specimen and the single edge notched bending specimen (SENB). In contrast, only a small difference between the J_R curve of the CT specimen and

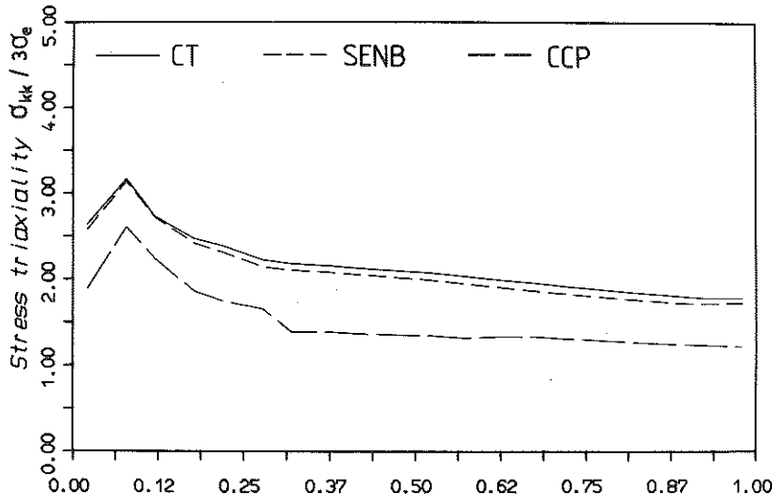

Fig 11 Distributions of the stress triaxiality ahead of the crack tip of different specimen configurations

the curve of the SENB-specimen was found. To explain the geometry dependence of the J_R curve the distributions of the stress triaxiality $\sigma_{kk}/3\sigma_e$ ahead of the crack tip were plotted in Fig. 11 for the three specimen configurations under the same crack tip load $J = 50$ kJ/m^2. The CCP specimen shows the lowest stress triaxiality in comparison with the CT and SENB specimens. Since the voids grow faster with increasing stress triaxiality, an earlier crack initiation by void coalescence and also a lower resistance against the crack extension could be expected for the CT and SENB specimen. It is well known from many experiments that the CCP specimen delivers a steeper J_R curve than the specimens with considerable bending moments like the CT and SENB specimens.

Conclusions

The parameters for the application of the modified Gurson model can partly be determined by quantitative metallography. The remaining parameter f_c is obtained by comparing numerical and experimental load versus displacement curves for the smooth bar. The fracture behaviour of notched bars with different notch radii was simulated very accurately using the parameters obtained from the smooth bar.

For the analysis of cracked structures the ctitical distance l_c becomes important. Reasonable variations of J resistance curves were predicted on the basis of the modified Gurson model for different cracked specimen configurations using the parameters obtained from the smooth bar and the l_c value determined from the CT-specimen.

Acknowledgements

The authors are grateful to the Deutsche Forschungsgemeinschaft (German Science Foundation) who supports these investigations.

References

(1) SUN, D.-Z., DORMAGEN, D., and DAHL, W. (1985) *Steel Research*, **56**, 445–449.
(2) AURICH, D. and SOMMER, E. (1988) *Steel Research*, **59**, 358–367.
(3) NEEDLEMAN, A. and TVERGAARD, V. (1984) *J. Mech. Phys. Solids*, **32**, 461–490.
(4) GURSON, A. L. (1977) *J. Engng. Mat. Tech.*, **99**, 2–15.
(5) NEEDLEMAN, A. and TVERGAARD, V. (1987) *J. Mech. Phys. Solids*, **35**, 151–183.
(6) BECKER, R., NEEDLEMAN, A., SURESH, S., TVERGAARD, V., and VASUDEVAN, A. K. (1989) *Acta Metall.*, **37**, 99–120.
(7) TVERGAARD, V. (1982) *Int. J. Fract.*, **18**, 237–252.
(8) CHU, C. C. and NEEDLEMAN, A. (1980) *J. Engng. Mat. Techn.*, **102**, 249–256.
(9) ARAVAS, N. and McMEEKING, R. M. (1985) *Int. J. Fract.*, **29**, 21–38.
(10) SUN, D.-Z., SIEGELE, D., VOSS, B., and SCHMITT, W. (1988) *Fatigue Fracture Engng. Mater. Structures*, **12**, 201–212.
(11) BRIDGMAN, P. W. (1952) *Studies in large flow and fracture*, New York.
(12) SUN, D.-Z., VOSS, B., and SCHMITT, W. (1988) *Vorträge der 20*, Sitzung des DVM–Arbeitskreises Bruchvorgänge, Frankfurt, 479–490.